Current Sheets and Collisionless Damping in Kinetic Plasma Turbulence

J. M. TenBarge
jason-tenbarge@uiowa.edu
Department of Physics and Astronomy, University of Iowa, Iowa City, IA 52242, USA

G. G. Howes
Department of Physics and Astronomy, University of Iowa, Iowa City, IA 52242, USA.

ABSTRACT

We present the first study of the formation and dissipation of current sheets at electron scales in a wave-driven, weakly collisional, 3D kinetic turbulence simulation. We investigate the relative importance of dissipation associated with collisionless damping via resonant wave-particle interactions versus dissipation in small-scale current sheets in weakly collisional plasma turbulence. Current sheets form self-consistently from the wave-driven turbulence, and their filling fraction is well correlated to the electron heating rate. However, the weakly collisional nature of the simulation necessarily implies that the current sheets are not significantly dissipated via Ohmic dissipation. Rather, collisionless damping via the Landau resonance with the electrons is sufficient to account for the measured heating as a function of scale in the simulation, without the need for significant Ohmic dissipation. This finding suggests the possibility that the dissipation of the current sheets is governed by resonant wave-particle interactions and that the locations of current sheets correspond spatially to regions of enhanced heating.

Subject headings: turbulence — plasmas — solar wind

1. Introduction

Turbulence plays an important role in space and astrophysical plasmas by mediating the transfer of energy from large-scale motions to the small scales at which the turbulence can be dissipated. A major unsolved problem is the identification of the physical mechanisms that dissipate the small-scale turbulent motions, ultimately converting the turbulent energy to plasma heat. The dynamics at the dissipative scales are typically weakly collisional in diffuse astrophysical plasmas, such as the solar wind, so the mechanisms responsible for the dissipation and plasma heating are described by kinetic plasma physics. Two mechanisms have been proposed to be the dominantly involved in the dissipation process for plasma turbulence: collisionless wave-particle interactions (Howes et al. 2008a; Schekochihin et al. 2009; TenBarge et al. 2013a) and dissipation in small-scale current sheets (Dmitruk et al. 2004; Markovskii & Vasquez 2011; Matthaeus & Velli 2011; Osman et al. 2011a; Servidio et al. 2011; Karimabadi et al. 2013).

In weakly collisional plasmas, it is well known that wave-particle interactions lead to significant collisionless damping of the linear kinetic wave modes via the Landau and cyclotron resonances. In turbulent astrophysical plasmas, it has been proposed that the fluctuations at perpendicular scales smaller than the ion Larmor radius, $k_\perp \rho_i \gtrsim 1$, have properties typical of kinetic Alfvén waves (Howes et al. 2008b,a; Howes 2008; Schekochihin et al. 2009; Salem et al. 2012), and will therefore suffer collisionless damping. In the case of the solar wind, it has been sug-

gested (Howes et al. 2008a; Schekochihin et al. 2009; Howes et al. 2011a,b) that electron Landau damping dominates the dissipation of these turbulent electromagnetic fluctuations at $k_\perp \rho_i \gtrsim 1$. Free energy transferred conservatively to the particle distribution functions by wave-particle interactions is ultimately thermalized by arbitrarily weak collisions through the action of an entropy cascade in phase space (Schekochihin et al. 2009). Adopting this paradigm, predictive cascade models of the plasma turbulence and its dissipation can be constructed by assuming that the collisionless damping rates of the turbulent electromagnetic fluctuations are related to the linear damping rates from kinetic theory (Howes et al. 2008a, 2011b).

On the other hand, a number of recent studies focusing on the intermittent structures that inherently develop in plasma turbulence have suggested that dissipation dominantly occurs in coherent structures, in particular, small-scale current sheets (Dmitruk et al. 2004; Markovskii & Vasquez 2011; Matthaeus & Velli 2011; Osman et al. 2011a; Servidio et al. 2011; Karimabadi et al. 2013). The kinetic physical mechanism by which dissipation occurs in current sheets has not been elucidated. Hybrid kinetic-ion and fluid-electron simulations in 2D suggest perpendicular ion heating in current sheets (Parashar et al. 2009; Markovskii & Vasquez 2011), 2D and 3D Particle-in-Cell (PIC) simulations of reconnection suggest the acceleration of electrons by parallel electric fields (Pritchett 2006; Egedal et al. 2008, 2009; Le et al. 2010; Egedal et al. 2010, 2012), and 2D gyrokinetic simulations suggest linear phase mixing/Landau damping (Loureiro et al. 2013). Temperature measurements in the near-Earth solar wind have been used to both support (Osman et al. 2011a,b) and refute (Borovsky & Denton 2011) the proposal that plasma heating dominantly occurs in current sheets.

In this Letter, we present a wave-driven, 3D gyrokinetic turbulence simulation at scales smaller than the ion Larmor radius that self-consistently generates small-scale current sheets. We find that the current sheet filling fraction is well correlated with the electron heating rate in the simulation. Yet, Ohmic dissipation is negligible, and the measured electron heating rate by scale is well reproduced by assuming dissipation is entirely associated with electron Landau damping, suggesting the possibility that the current sheets are damped collisionlessly by resonant wave-particle interactions and correspond to regions of local heating.

2. Kinetic Simulation

The simulation was performed with the Astrophysical Gyrokinetics code, `AstroGK` (Numata et al. 2010), a triply periodic Eulerian slab code that solves the five-dimensional, electromagnetic gyroaveraged Vlasov-Maxwell equations for the perturbed gyroaveraged distribution for each species and the gyroaveraged Maxwell's equations (Frieman & Chen 1982; Howes et al. 2006). Collisions are treated using a fully conservative, linearized, and gyroaveraged collision operator (Abel et al. 2008; Barnes et al. 2009). The simulations are driven at the simulation domain scale with an oscillating Langevin antenna coupled to the component of the vector potential parallel to the equilibrium magnetic field, $\mathbf{B}_0 = B_0 \hat{\mathbf{z}}$ (TenBarge et al. 2013b).

The simulation models a proton and electron plasma with a realistic mass ratio $m_i/m_e = 1836$, $\beta_i = 1$, and $T_i/T_e = 1$, where $\beta_i = v_{ti}^2/v_A^2$, v_A is the Alfvén speed, and $v_{ti} = \sqrt{2T_i/m_i}$ is the ion thermal speed. The simulation employs a periodic domain of size $L_\perp^2 \times L_z$, elongated along the straight, uniform equilibrium magnetic field $\mathbf{B}_0$. Relevant parameters for the simulation are $k_\perp \rho_i \in [5, 105]$, $k_z \rho_i/\epsilon \in [1, 16]$, $A_0/\epsilon \rho_i B_0 = 0.2$, $\nu_i \rho_i / v_{ti} \epsilon = 0.2$, and $\nu_e \rho_i / v_{ti} \epsilon = 0.5$, where $\rho_i = v_{ti}/\Omega_i$ is the ion Larmor radius, Ω_i is the ion gyrofrequency, $\epsilon = 2\pi\rho_i/L_z = 0.081 \ll 1$ is the gyrokinetic expansion parameter, A_0 is the antenna amplitude, and ν_s is the collision frequency of species s. Time is normalized to the linear frequency, determined by the collisionless gyrokinetic dispersion relation (Howes et al. 2006), of a kinetic Alfvén wave at the simulation domain scale, $\omega_0 = 3.6 k_{z0} v_A = 3.6 \omega_{A0}$. Therefore, the corresponding domain scale turn-around time is $\tau_0 = 2\pi/\omega_0 \simeq 1.75 \omega_{A0}^{-1}$. Collision frequencies are chosen to prevent build-up of small-scale structure in velocity space but remain small enough not to alter the weakly collisional dynamics: $\nu_s \ll \omega_0$ is satisfied, so the simulation is weakly collisional. The expansion parameter ϵ sets the parallel domain size, determined by assuming a critically balanced cascade driven isotropically

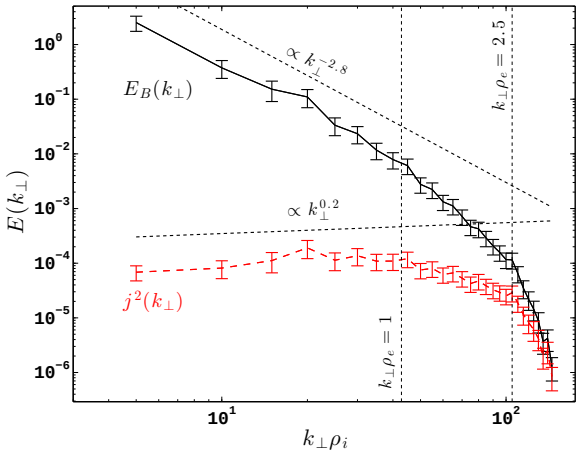

Fig. 1.— (Color online) Time averaged one-dimensional trace magnetic energy spectrum (solid) and the spectrum of the square of the current density (dashed).

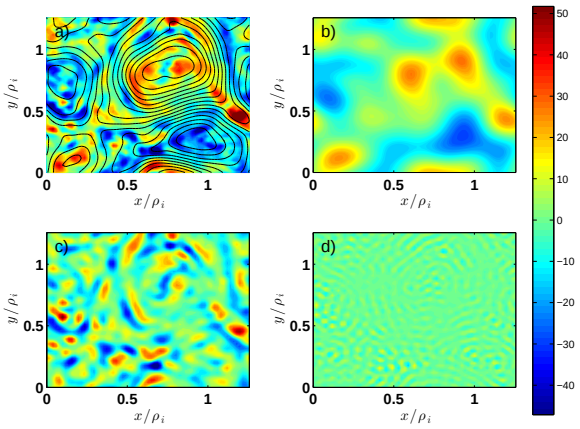

Fig. 2.— (Color online) Parallel current density, j_z, for a perpendicular plane at $t = 2.43\tau_0$, with different band-pass filters applied: (a) unfiltered, (b) $5 \leq k_\perp\rho_i < 21$, (c) $21 \leq k_\perp\rho_i < 84$, and (d) $k_\perp\rho_i \geq 84$. Contours of the parallel vector potential A_z are shown in (a).

at the energy injection scale, $k_i\rho_i = 10^{-4}$, chosen to model solar wind turbulence (Howes et al. 2008a). The antenna amplitude is chosen to satisfy critical balance at the domain scale, so the simulation represents critically balanced, strong turbulence. Prior analysis of a similar simulation (TenBarge et al. 2013a) demonstrates a magnetic energy spectrum in excellent agreement with the empirical form found from a large statistical sample of dissipation range measurements in the solar wind (Alexandrova et al. 2012).

3. Magnetic Energy Spectrum and Current Density Spectrum

First we demonstrate that the magnetic energy spectrum from our simulation is consistent with measurements in the solar wind, and then present the perpendicular wavenumber spectrum of the square of the current density, $j^2(k_\perp)$. In Figure 1, we plot (solid) the average one-dimensional trace magnetic energy spectrum $E_B(k_\perp)$, where the total magnetic energy $E_B^{(tot)} = \int dk_\perp E_B(k_\perp)$. The average is performed over the steady-state evolution of the system, $1.5\tau_0 \leq t \leq 4.1\tau_0$; error bars represent the variance over the same interval. This spectrum is quantitatively consistent with a large sample of measurements of the dissipation range magnetic energy spectrum in the solar wind (Alexandrova et al. 2012), suggesting that this simulation contains the essential physical ingredients underlying turbulence in the solar wind. Since $j = |\mathbf{j}| = |(c/4\pi)\nabla \times \mathbf{B}|$, we expect to find $j \propto kB$, and therefore the scaling of $j^2(k_\perp) = \int k_\perp d\phi dk_\parallel j^2(\mathbf{k})$ should satisfy the relation $j^2(k_\perp) \propto k_\perp^3 E_B(k_\perp)$, as confirmed by the plotted spectrum (dashed) of $j^2(k_\perp)$.

4. Current Sheet Formation

In a weakly collisional plasma, magnetic reconnection in the presence of a guide magnetic field is expected to develop an electron diffusion region at the scale $k_\perp\rho_e \sim 1$ (Birn & Priest 2006), where a strong current sheet is expected to form. In Figure 2, we plot (a) the parallel current density $j_z(x, y)$ from a perpendicular cut through the simulation domain. To explore the contribution to the current from different scales, we present spatially band-pass filtered data: (b) $5 \leq k_\perp\rho_i < 21$, (c) $21 \leq k_\perp\rho_i < 84$, and (d) $k_\perp\rho_i \geq 84$. The large-scale currents visible in panels (a) and (b) are dominated by the driving, which generates upward and downward propagating kinetic Alfvén waves with $k_\perp\rho_i = 5$. Panel (c), whose filter is approximately centered on the electron gyroradius, $0.49 \leq k_\perp\rho_e \leq 1.95$, shows that this 3D gyrokinetic simulation indeed produces current sheets

at the ρ_e scale, consistent with such development in a wide range of plasma turbulence simulations. These electron-scale diffusion regions are highly intermittent, both spatially and temporally, with a typical lifetime $\tau \lesssim 0.1\tau_0$. The lack of significant current density in panel (d) shows that current sheets do not form at scales $k_\perp \rho_e > 2$, confirming that our simulation has sufficient perpendicular spatial resolution to capture fully the current sheet dynamics.

Note that we are using the general definition of current sheet as a tangential discontinuity in the magnetic field, e.g., Parker (1994); Birn & Priest (2006). This is also consistent with the definition of current sheet used in recent solar wind literature, e.g., Vasquez et al. (2007); Greco et al. (2009); Osman et al. (2011a). We do not attempt differentiate between current sheets associated with reconnecting magnetic flux and those arising from interfering Alfvén waves.

It is also important to note that the simulation is driven by injecting domain-scale waves, which generate strong turbulence. The current sheets form self-consistently from the cascade of wave-driven turbulence and are not seeded or otherwise initialized to form. Therefore, we conclude that electron-scale current sheets form as a natural consequence of Alfvénic turbulence in this 3D gyrokinetic simulation.

5. Current Sheets and Electron Heating

We next examine the relative contribution to the measured electron heating from wave-particle interactions and dissipation in current sheets. The analytical equations for plasma heating (Howes et al. 2006) have been implemented as a diagnostic in `AstroGK`. Boltzmann's H Theorem states that the entropy increase necessary for irreversible heating requires collisions (Howes et al. 2006), so the collisional heating (plus a small amount of numerical dissipation) is used to measure the heating rate of each plasma species. Over the range of scales simulated, $k_\perp \rho_i \in [5, 105]$, little ion heating occurs, so we focus on the electron heating. The collisional electron heating is given by

$$Q_e = -\sum_{\mathbf{k}_\perp} \int_{-L_z}^{L_z} \frac{dz}{2L_z} \int d^3\mathbf{v} \frac{T_{0e}}{F_{0e}} \left[h_{e\mathbf{k}_\perp} \left(\frac{\partial h^*_{e\mathbf{k}_\perp}}{\partial t} \right)_{\text{coll}} + h^*_{e\mathbf{k}_\perp} \left(\frac{\partial h_{e\mathbf{k}_\perp}}{\partial t} \right)_{\text{coll}} \right] \quad (1)$$

where $h_{e\mathbf{k}_\perp} = h_e(k_x, k_y, z, v_\parallel, v_\perp, t)$ is the non-Boltzmann portion of the perturbed electron distribution function and F_{0e} is the equilibrium electron distribution function (Howes et al. 2006; Numata et al. 2010). The collisional electron heating as a function of perpendicular wavenumber $Q_e(k_\perp)$ is computed by summing over annular rings in the perpendicular plane such that the total heating is given by $Q_e = \int dk_\perp Q_e(k_\perp)$. Note that, in the weakly collisional limit, the heating rate is independent of the collision frequency (Howes et al. 2006). For the steady-state evolution of the simulation over $1.5\tau_0 \leq t \leq 4.1\tau_0$, the heating diagnostics recover total power balance to $\lesssim 2\%$ (TenBarge et al. 2013a).

To estimate the contribution of current sheet dissipation to the heating rate, we compare the fraction of volume occupied by current sheets to the electron heating rate as a function of time. The volume filling fraction of current sheets is computed as the percentage of the volume with current density $j > j_{th}$, with a chosen threshold $j_{th} = j_{max}/3$, where j_{max} is the maximum current density over all time and space in the simulation. Note that varying this threshold alters the magnitude of the filling fraction but not the form of its variation with time. In Figure 3 a), we plot the volume filling fraction in percent (black dashed) and the electron collisional heating rate, discussed above, Q_e (red solid) as a function of time—all quantities in the figure have been integrated over the entire simulation domain. In Figure 3 b) is plotted the boxcar averaged (over $\Delta t = 0.13\tau_0$) power injected into the plasma by the Langevin antenna (magenta dotted) and the total energy of the turbulent fluctuations in the simulation including the magnetic field and kinetic energies $E_{KAW} = E_{B_\perp} + E_{B_\parallel} + E_{KE}$ (blue dash-dotted), where $E_{KE} = \sum_s m_s n_{0s} u_s^2/2$ and $\mathbf{u}_s$ is the fluid velocity of each species.

The cross correlations between the electron heating rate and filling fraction (black solid), antenna power (magenta dotted), and E_{KAW} (blue dash-dotted) are plotted in Figure 3 c). The injected antenna power and the electron heating rate are poorly correlated, $\langle \max(\text{Corr}(Q, j_{ant})) \rangle = 0.52 \pm 0.02$—the mean and variance are calcu-

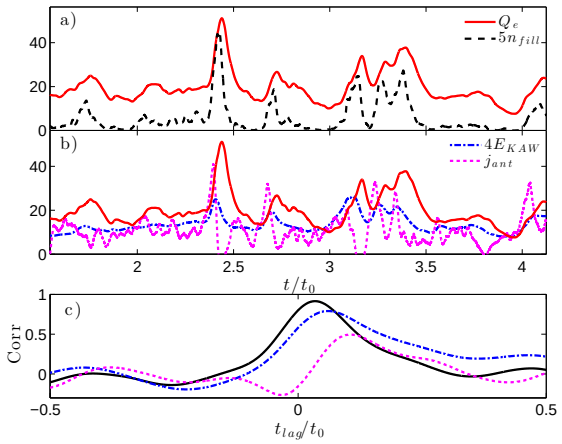

Fig. 3.— (Color online) a) Volume filling fraction of current sheets satisfying $j > j_{max}/3$ in percent (black dashed) and the electron collisional heating rate Q_e (red solid). b) The injected antenna power (magenta dotted) and the total turbulent energy, E_{KAW}, (blue dash-dotted). c) Cross correlations between the electron heating rate and filling fraction (black solid), antenna power (magenta dotted), and E_{KAW} (blue dash-dotted).

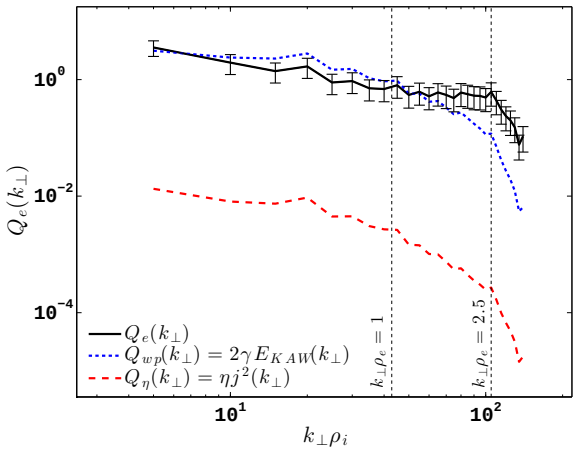

Fig. 4.— (Color online) Measured heating of the electrons from the simulation by perpendicular wavenumber, $Q_e(k_\perp)$ (solid), an estimate of the electron heating based on linear wave-particle damping $Q_{wp}(k_\perp)$ (dotted), and the Ohmic heating rate $Q_\eta(k_\perp)$ (dashed).

lated from the present simulation and five other identically prepared simulations employing different random number seeds for the turbulent driving. Similarly, the electron heating rate and total turbulent energy are not well correlated, $\langle \max(\mathrm{Corr}(Q, E_{KAW})) \rangle = 0.78 \pm 0.04$, suggesting that the heating rate is not simply a function of the driving or magnitude of turbulent energy. On the other hand, the electron heating rate is well correlated with the current sheet filling fraction, $\langle \max(\mathrm{Corr}(Q, n_{fill})) \rangle = 0.91 \pm 0.04$. The strong correlation suggests that dissipation associated with current sheets plays an important role in heating the electrons.

6. Electron Heating by Scale

In Figure 4, we present a plot of the electron collisional heating rate by perpendicular wavenumber, $Q_e(k_\perp)$ (solid), averaged over $1.5\tau_0 \leq t \leq 4.1\tau_0$, where error bars represent the variance over the interval. Note that the instantaneous shape of this heating curve is similar to the average, and does not change significantly as current sheets form and dissipate. This plot shows that the electron heating is nearly constant over all scales, with about half of the total heating occurring at scales $k_\perp\rho_e < 1$. The turn-down at $k_\perp\rho_i > 105$ is an artifact due to the diminishing number of Fourier modes in the corner beyond the fully resolved simulation domain.

As a function of $k_\perp$, we may predict the collisionless damping of the turbulent fluctuations by resonant wave-particle interactions in our simulation using $Q_{wp}(k_\perp) = 2\gamma(k_\perp)E_{KAW}(k_\perp)$, where γ is the *linear* kinetic damping rate of kinetic Alfvén waves (dominated by electron Landau damping). This prediction for the wave-particle interaction heating rate requires integration over $k_\parallel$, where parallel is with respect to the local magnetic field and is typically determined via structure functions or wavelets. To avoid the complications of determining the local magnetic field direction, we use frequency as a proxy for the parallel wave vector since $\omega \propto k_\parallel$ for kinetic Alfvén waves—an approach also taken in TenBarge & Howes (2012). This prediction for wave-particle damping, plotted in Figure 4 (dotted), admits *no free parameters*, yet it agrees quite well with the measured collisional electron heating (solid): the integrated, total predicted electron heating is within 4% of the collisional heating diagnosed in AstroGK. The

slight excess of wave-particle damping at $5 < k_\perp \rho_i < 40$ and excess of electron collisional heating at $k_\perp \rho_i > 40$ is consistent with the action of the electron entropy cascade (Schekochihin et al. 2009). Through the entropy cascade, energy removed by electron Landau damping at $5 < k_\perp \rho_i < 40$ is expected to appear as collisional heating at higher wavenumbers, consistent with the simulation results in Figure 4.

We also compute the Ohmic heating rate $Q_\eta = \eta j^2$, where $\eta = 0.38(4\pi)\nu_{ei} d_e^2/c^2$ is the Spitzer resistivity (Spitzer & Härm 1953), $\nu_{ei} = \nu_e$ is the electron-ion collision frequency, $d_e = c/\omega_{pe}$ is the electron inertial length, and ω_{pe} is the electron plasma frequency. The Ohmic heating rate is plotted (dashed) in Figure 4, falling well below the measured heating rate and the predicted collisionless damping rate, $Q_\eta \ll Q_{wp} \simeq Q_e$. Theory predicts negligible Ohmic heating for a weakly collisional plasma, since electron-ion collisions are insufficient to significantly heat the electrons. Therefore, Ohmic dissipation of the current cannot account for the observed electron heating in the simulation, despite the strong correlation between current sheet filling fraction and heating rate.

7. Discussion

A puzzling aspect of these results is that, despite the clear correlation between the electron heating rate and the volume filling fraction of current sheets, the electron heating as a function of wavenumber is well predicted assuming that Landau damping is entirely responsible for the electron heating. This unexpected agreement raises the interesting possibility that the dissipation of the current sheets in the simulation occurs entirely via Landau damping.

The solution to this puzzle lies in the relationship between the current and magnetic field, namely $j \propto kB$. This relationship implies that regions of strong current correspond to regions with enhanced small-scale magnetic structure since the current is weighted toward small spatial scales. Since the linear kinetic damping rate increases with wavenumber, regions with enhanced small-scale magnetic structure will also correspond to regions of enhanced wave-particle damping. Therefore, regions of strong current may also correspond

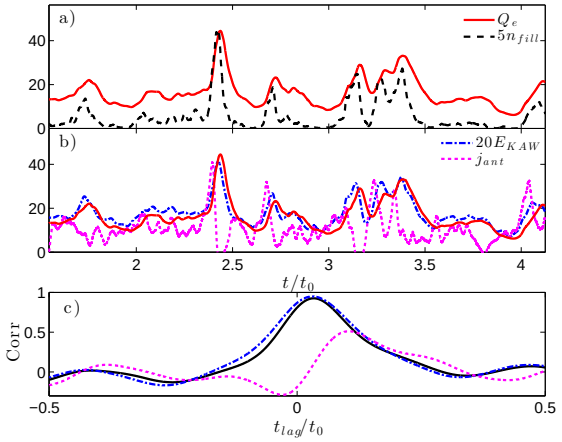

Fig. 5.— (Color online) Quantities as in Figure 3 with a high-pass filter applied to remove modes with $k_\perp \rho_i < 10$, except the antenna current.

to regions of enhanced wave-particle damping.

To test this hypothesis, we apply a high-pass filter to the data presented in Figure 3 retaining only modes with $k_\perp \rho_i \geq 10$—no filter is applied to the antenna current. The result of the filtering is plotted in Figure 5, where all of the cross correlations exceed 0.9, with the exception of the antenna power, which remains poorly correlated.

The picture suggested by this simulation is one in which current sheets are self-consistently formed by the interaction of kinetic Alfvén wave-like fluctuations, where each of the fluctuations is dissipating at its Landau damping rate. Therefore, current sheet formation and dissipation is dominated by the evolution of the Alfvénic turbulence, and current sheets correspond to sites of enhanced dissipation and heating, as suggested by recent analyses of solar wind turbulence (Osman et al. 2011a,b).

8. Conclusion

For a wave-driven, 3D gyrokinetic simulation of the dissipation range, $k_\perp \rho_i \in [5, 105]$, we find that current sheets self-consistently develop, in qualitative agreement with fluid simulations. The electron heating rate is well correlated with the volume filling fraction of current sheets, suggesting that the dissipation of current sheets plays an important role in the heating of electrons. However, the electron heating rate as a function of scale

is well predicted by assuming that all dissipation is due to collisionless damping of the turbulent fluctuations via Landau resonance with the electrons. In the weakly collisional plasma, Ohmic dissipation of current sheets is negligible. Due to the relationship between the current and magnetic field, significant current highlights regions with enhanced small-scale magnetic structure, which will be collisionlessly damped at a rate greater than surrounding plasma. This suggests that current sheets may correspond spatially to locations of enhanced dissipation and heating, regardless of whether that dissipation is due to collisionless wave-particle interactions or active magnetic reconnection.

The authors thank Homa Karimabadi for helpful suggestions. This work was supported by NASA grant NNX10AC91G and NSF CAREER grant AGS-1054061. This research used resources of the Oak Ridge Leadership Computing Facility, supported by the Office of Science of the U.S. DOE under Contract No. DE-AC05-00OR22725. This research was supported by an allocation of advanced computing resources provided by the NSF, partly performed on Kraken at the National Institute for Computational Sciences.

REFERENCES

Abel, I. G., Barnes, M., Cowley, S. C., Dorland, W., & Schekochihin, A. A. 2008, Phys. Plasmas, 15, 122509

Alexandrova, O., Lacombe, C., Mangeney, A., Grappin, R., & Maksimovic, M. 2012, ApJ, 760, 121

Barnes, M., Abel, I. G., Dorland, W., et al. 2009, Phys. Plasmas, 16, 072107

Birn, J., & Priest, E. R., eds. 2006, Reconnection of Magnetic Fields (Cambridge University Press)

Borovsky, J. E., & Denton, M. H. 2011, ApJ, 739, L61

Dmitruk, P., Matthaeus, W. H., & Seenu, N. 2004, ApJ, 617, 667

Egedal, J., Daughton, W., Drake, J. F., Katz, N., & Lê, A. 2009, Phys. Plasmas, 16, 050701

Egedal, J., Daughton, W., & Le, A. 2012, Nature Physics, 8, 321

Egedal, J., Fox, W., Katz, N., et al. 2008, J. Geophys. Res., 113, 12207

Egedal, J., Lê, A., Zhu, Y., et al. 2010, Geophys. Res. Lett., 37, 10102

Frieman, E. A., & Chen, L. 1982, Phys. Fluids, 25, 502

Greco, A., Matthaeus, W. H., Servidio, S., Chuychai, P., & Dmitruk, P. 2009, ApJ, 691, L111

Howes, G. G. 2008, Phys. Plasmas, 15, 055904

Howes, G. G., Cowley, S. C., Dorland, W., et al. 2006, ApJ, 651, 590

—. 2008a, J. Geophys. Res., 113, A05103

Howes, G. G., Dorland, W., Cowley, S. C., et al. 2008b, Phys. Rev. Lett., 100, 065004

Howes, G. G., TenBarge, J. M., & Dorland, W. 2011a, Phys. Plasmas, 18, 102305

Howes, G. G., TenBarge, J. M., Dorland, W., et al. 2011b, Phys. Rev. Lett., 107, 035004

Karimabadi, H., Roytershteyn, V., Wan, M., et al. 2013, Phys. Plasmas, 20, 012303

Le, A., Egedal, J., Daughton, W., et al. 2010, Geophys. Res. Lett., 37, 3106

Loureiro, N. F., Schekochihin, A. A., & Zocco, A. 2013, ArXiv e-prints

Markovskii, S. A., & Vasquez, B. J. 2011, ApJ, 739, 22

Matthaeus, W. H., & Velli, M. 2011, Space Sci. Rev., 160, 145

Numata, R., Howes, G. G., Tatsuno, T., Barnes, M., & Dorland, W. 2010, J. Comp. Phys., 229, 9347

Osman, K. T., Matthaeus, W. H., Greco, A., & Servidio, S. 2011a, ApJ, 727, L11

Osman, K. T., Matthaeus, W. H., Wan, M., & Rappazzo, A. F. 2011b, ArXiv e-prints

Parashar, T. N., Shay, M. A., Cassak, P. A., & Matthaeus, W. H. 2009, Phys. Plasmas, 16, 032310

Parker, E. N. 1994, Spontaneous current sheets in magnetic fields : with applications to stellar x-rays, Vol. 1 (Oxford University Press)

Pritchett, P. L. 2006, Geophys. Res. Lett., 33, 13104

Salem, C. S., Howes, G. G., Sundkvist, D., et al. 2012, ApJ, 745, L9

Schekochihin, A. A., Cowley, S. C., Dorland, W., et al. 2009, ApJS, 182, 310

Servidio, S., Dmitruk, P., Greco, A., et al. 2011, Nonlin. Proc. Geophys., 18, 675

Spitzer, L., & Härm, R. 1953, Phys. Rep., 89, 977

TenBarge, J. M., & Howes, G. G. 2012, Phys. Plasmas, 19, 055901

TenBarge, J. M., Howes, G. G., & Dorland, W. 2013a, ApJ, submitted

TenBarge, J. M., Howes, G. G., Dorland, W., & Hammett, G. W. 2013b, J. Comp. Phys., in preparation

Vasquez, B. J., Abramenko, V. I., Haggerty, D. K., & Smith, C. W. 2007, J. Geophys. Res., 112, 11102

This 2-column preprint was prepared with the AAS LaTeX macros v5.2.